Phases and domain structures in relaxor-based ferroelectric (PbMg1/3Nb2/3O3)0.69(PbTiO3)0.31 single crystal

Authors: C.-S. Tu, L.-F. Chen, V.H. Schmidt, and C.-L. Tsai

This is a postprint of an article that originally appeared in Japanese Journal of Applied Physics in 2001. The final version can be found at https://dx.doi.org/10.1143/JJAP.40.4118.

C.-S. Tu, L.-F. Chen, V.H. Schmidt, and C.-L. Tsai, “Phases and domain structures in relaxor-based ferroelectric (PbMg1/3Nb2/3O3)0.69(PbTiO3)0.31 single crystal,” Japanese Journal of Applied Physics 40, 4118-4125 (2001). doi: 10.1143/JJAP.40.4118

Phases and Domain Structures in Relaxor-Based Ferroelectric $(PbMg_{1/3}Nb_{2/3}O_3)_{0.69}(PbTiO_3)_{0.31}$ Single Crystal

Chi-Shun TU[1,*] Li-Fang CHEN[1], V. Hugo SCHMIDT[2] and Chih-Long TSAI[1]
[1]*Department of Physics, Fu Jen University, Taipei, Taiwan 242, Republic of China*
[2]*Department of Physics, Montana State University, Bozeman, MT 59717, USA*

(Received October 15, 2000; accepted for publication January 22, 2001)

The Brillouin back-scattering spectra, dielectric permittivities, polarization–electric field (P–E) hysteresis loops and domain structures have been measured as a function of temperature in a relaxor-based ferroelectric single crystal $(PbMg_{1/3}Nb_{2/3}O_3)_{0.69}(PbTiO_3)_{0.31}$ (PMN–31%PT). In order of increasing temperature, PMN–31%PT undergoes succes-sive phase transitions: rhombohedral phase (below $\sim$ 370 K) $\rightarrow$ coexistence of rhombohedral and tetragonal phases (between $\sim$ 370 and $\sim$ 380 K) $\rightarrow$ tetragonal phase (between $\sim$ 380 and $\sim$ 400 K) $\rightarrow$ coexistence of tetragonal and cubic phases (betwee $\sim$ 400 and $\sim$ 420 K) $\rightarrow$ cubic phase (above $\sim$ 420 K). An extra ferroelectric anomaly of the dielectric per-mittivity appears at 370 K possibly due to the percolating polar cluster induced by an external electric field. It was found that different individual domain regions have different transition temperatures. This phenomenon suggests an inhomogeneous dis-tribution of Ti^{4+} concentration in the PMN–31%PT crystal. The dielectric permittivity ε' of PMN–31%PT obeys the empirical relation, $\varepsilon'_m/\varepsilon^{\gamma}(f, T) = 1 + [T - T_m(f)]'/2\delta_{\gamma}^2$, above the temperature of permittivity maximum T_m.

KEYWORDS: relaxor-based ferroelectric, PMN–31%PT, phase transition, domain structure

1. Introduction

Relaxor ferroelectrics generally mean the complex perovskites with ABO_3-type unit cell and are crystals in which unlike-valence cations belonging to a given site (A or B) are presented in the correct ratio for charge balance, but are situated randomly on these cation sites.[1–4] These randomly different cation charges give rise to random fields, which tend to make the phase transitions "diffuse" instead of sharp as in normal ferroelectrics.[3,4] Lead magnesium niobate, $Pb(Mg_{1/3}Nb_{2/3})O_3$ (PMN), is one of the most interesting relaxor ferroelectric (FE) materials. PMN has a disordered complex structure in which the Mg^{2+} and Nb^{5+} cations exhibit only short range order on the B site. Near 280 K, the PMN crystal undergoes a diffuse phase transition (which is characterized by a broad frequency-dependent dielectric maximum) and has cubic symmetry at room temperature with space group *Pm3m*, whereas below 200 K a small rhombohedral distortion (pseudocubic) was observed.[1,5] The normal FE crystal $PbTiO_3$ (PT) has tetragonal symmetry with space group *P4mm* at room temperature and has a normal FE phase transition taking place at $T_c = 760$ K with long-range FE order occurring below T_c.[6]

The relaxor-based FE crystals $(PbMg_{1/3}Nb_{2/3}O_3)_{1-x}$-$(PbTiO_3)_x$ (PMN–xPT) are expected to show properties of both relaxor ferroelectric PMN and normal ferroelectric PT. PMN–xPT naturally has a morphotropic phase boundary (MPB) in the range of $\sim$28 to $\sim$36 mol% of PT.[7] In other words, as temperature decreases, the mixed crystals PMN–xPT ($0.28 \leq x \leq 0.36$) have successive phase transitions: cubic paraelectric (PE) phase $\rightarrow$ tetragonal FE phase $\rightarrow$ rhombohedral FE phase. The spontaneous deformations of the tetragonal state appear along the equivalent [001] directions, giving six fully ferroelectric domain states with the spontaneous polarization P_s and the optical axes (OA) oriented parallel to [001]. In the low temperature region, the crystals exhibit a polar rhombohedral phase with the P_s and the OA oriented along the [111] direction.

The engineered domain state that gives high piezoelectric response consists of {001}-cut crystals in the rhombohedral phase which when poled have all four of the eight ⟨111⟩-type domains, namely [111], [1$\bar{1}$1], [$\bar{1}$11], and [$\bar{1}\bar{1}$1], that have polarization components in the poling field direction. Paik *et al*. showed that a field of 20 kV/cm in PZN–8%PT destroys the rhombohedral state and induces a single tetragonal domain.[8] By *in situ* X-ray diffraction during field application, Durbin *et al*. confirmed that this field-induced crystallographic change occurs.[9] By optical microscopy, with field applied along {001}, Belegundu *et al*. confirmed that tetragonal and rhombohedral domains coexist at room temperature and even down to -100°C.[10] Perhaps the strain caused by the presence of the above four types of ⟨111⟩ domains is partly relieved by the presence of tetragonal ⟨001⟩ domains induced by the external dc field.

Single crystals of PMN–PT have been reported to exhibit much larger piezoelectric constants and electromechanical coupling factors compared with those in the $PbZrO_3$–$PbTiO_3$ (PZT) family of ceramics.[11–13] Such high piezoelectric performance, which converts mechanical and electric energies, is crucial in medical imaging, telecommunication and ultrasonic devices and may revolutionize these applications.[14] Many works have been undertaken on the growth and characterization of relaxor-based ferroelectrics.[15–21] However, limited attention has been paid to fundamental physical issues in these crystals, such as phase transitions and mesoscopic domain structures. It is believed that the phase coexistence and domain structure near the MPB play an important role in the high electro-mechanical coupling effect. Therefore, to have better understanding of phase transitions and domain structures, we carried out temperature-dependent measurements of Brillouin light scattering, dielectric permittivity, polarization–electric field (P–E) hysteresis loops and polarized light microscopy on a PMN–31%PT single crystal. The principles of optical crystallography and crystal symmetry were applied to analyze domain structures.

2. Experimental

The lead magnesium niobate-lead titanate single crystal PMN–31%PT (from H.C. Materials Co.), was grown using a modified Bridgman method with bottom seed.[15] The sample was cut perpendicular to the {001} direction. Here, direction "{ }" refers to the pseudocubic axes. The longitudinal acoustic (LA) phonon spectra were obtained from Brillouin back-scattering. The sample was illuminated along the {001} direction with an *Innova 90 plus-A3* argon laser with wavelength $\lambda = 514.5$ nm. The transverse acoustic (TA) mode was not observed in this report. Scattered light was analyzed by a Burleigh five-pass Fabry-Perot interferometer. The free spectral range of the Fabry-Perot interferometer was determined from measuring the LA phonon shift of fused quartz. Due to the low optical transmission and weak intensity factor, the signal/noise (S/N) ratio of the LA phonon spectra is about 2–3 for PMN–31%PT crystal, even though the S/N ratio from the fused quartz is greater than 60. The Brillouin scattering data were taken during a heating sequence.

For measurements of dielectric permittivity and P–E hysteresis loop, the sample surfaces were coated with silver paste electrodes. The electrode thickness is about 35 μm. The applied electric field was along the {001} direction. A variable-frequency *Wayne-Kerr Precision Analyzer Model PMA3260A* with four-lead connections was used to obtain capacitance and resistance. The heating/cooling rate for dielectric measurement was 1.5 K/min. For the field-cooled-zero-field-heated (FC-ZFH) dielectric measurement, the PMN–31%PT sample was first cooled from the cubic PE state (above 470 K) through phase transitions to room temperature with a dc bias field of $E = 4$ kV/cm along the {001} direction. Then the dielectric permittivity was measured upon heating without a bias field. The P–E hysteresis loops were measured by using a Sawyer-Tower circuit, at a frequency of 47 Hz. A *Janis Model CCS-450* closed-cycle refrigerator was used with a *Lakeshore Model 340* temperature controller.

Domain structures of the PMN–31%PT platelet were studied by using a *Nikon Model E600POL* polarized light microscope. The sample was cut perpendicular to the pseudocubic {001} direction and was finely polished. In order to minimize superposition of domains, the sample thickness was less than 100 μm. A *Linkam Model THMS600* heating/cooling stage mounted on the microscope was used for studying domain structures as a function of temperature. Domain structures were observed between a parallel polarizer-analyzer pair along the {001} direction, using a quarter-wave plate. In the tetragonal phase, adjacent domains can be polarized at 90° to each other and form strip-like domain walls.[22] Due to strain birefringence and total reflection at the boundary, the 90° domain wall is usually visible in polarized light. Thus, the tetragonal phase is usually characterized by superimposed domains with mutually perpendicular strips oriented along the {110} direction. Also, in the tetragonal state, adjacent domains can be polarized anti-parallel to each other and form the 180° domain walls that usually can not be observed with the polarizing microscope due to the same spontaneous strain in anti-parallel domains.[22] In the rhombohedral phase, when observing the {001} cut of platelet between crossed polarizers, the cross section of the optical indicatrix will exhibit extinction directions parallel to {110}.[21]

3. Results and Discussion

Actual LA phonon spectra for three selected temperatures are given in Fig. 1. The solid lines are fits to the damped harmonic oscillator model,[23] from which the phonon frequency shift and half-width (damping) were obtained. The acoustic phonon frequency exhibits a clear tendency to change with temperature. Figure 2 shows the temperature dependences of the phonon frequency, half-width and the real part ε' of dielectric permittivity. The phonon frequency of PMN–31%PT exhibits a broad minimum dip located near 395 K which corresponds to a broad damping maximum.

Figure 3 shows the temperature dependences of the real ε' and imaginary ε'' parts of the dielectric permittivity. Compared with the prototypical relaxor PMN, the dielectric permittivity ε' of PMN–31%PT shows a similar frequency-dependent diffuse phase transition with much higher values of $\varepsilon'_{\mathrm{m}} \sim 3 \times 10^4$ and $T_{\mathrm{m}} \sim 400$ K. T_{m} corresponds to the temperature giving maximum value $\varepsilon'_{\mathrm{m}}$ of the dielectric permittivity. In addition, near 380 K both the ε' and ε'' of PMN–31%PT exhibit an extra shoulder (as indicated by the downward arrow in Figure 3) which is superimposed on the broad dielectric background. Figure 4 illustrates the temperature-dependent data of ε' from cooling and heating processes. The inset of Figure 4 gives the reciprocal behavior of ε'. A clear thermal hysteresis was observed in a wide temperature region between ~300 and ~375 K. However, a weak thermal hysteresis was also seen in the region of ~390–400 K. Thermal hysteresis behavior implies a metastable state near the transition temperature, which can only exist theoretically for first- but not second-order transitions.

P–E hysteresis loops of PMN–31%PT are shown in

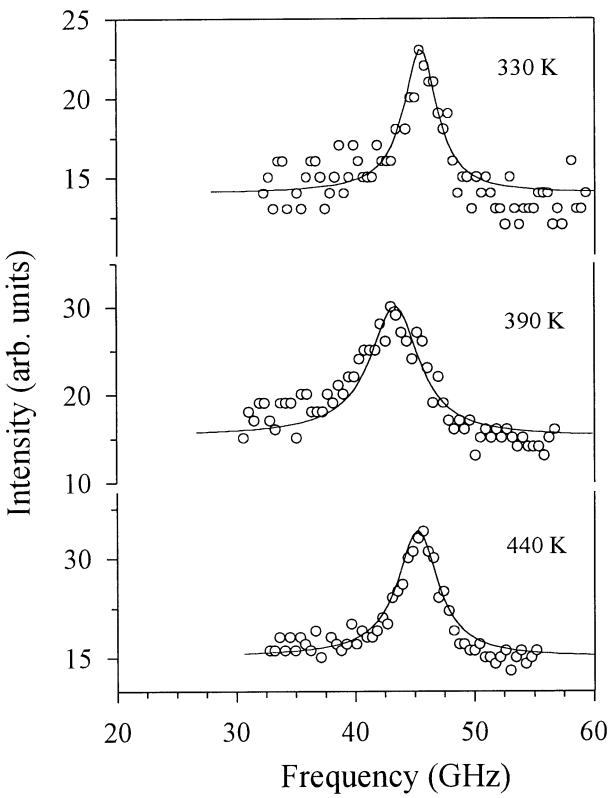

Fig. 1. Actual Brillouin scattering spectra for PMN–31%PT. The solid lines are fits to the damped harmonic oscillator model (ref. 23).

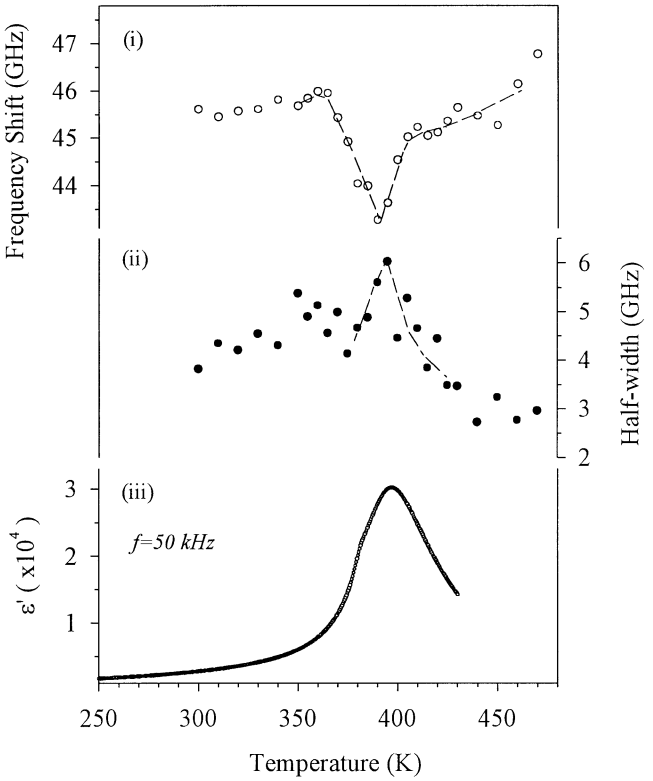

Fig. 2. (i) Brillouin frequency shift, (ii) half-width and (iii) the real part ε' of dielectric permittivity vs temperature. The dielectric data are taken at measuring frequency $f = 50$ kHz upon heating. The dashed lines are guides for the eye.

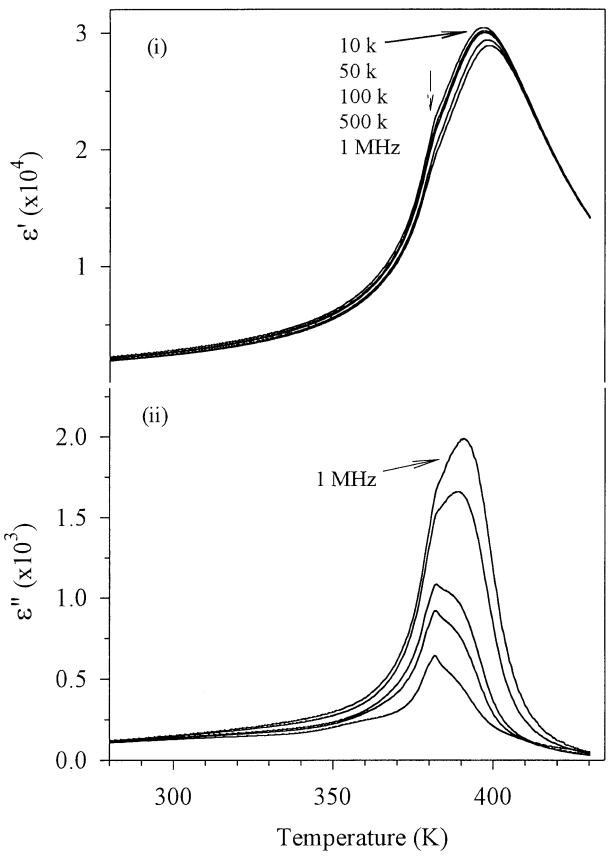

Fig. 3. Temperature dependences of (i) ε' and (ii) ε'' taken from frequencies 10 kHz–1 MHz upon heating.

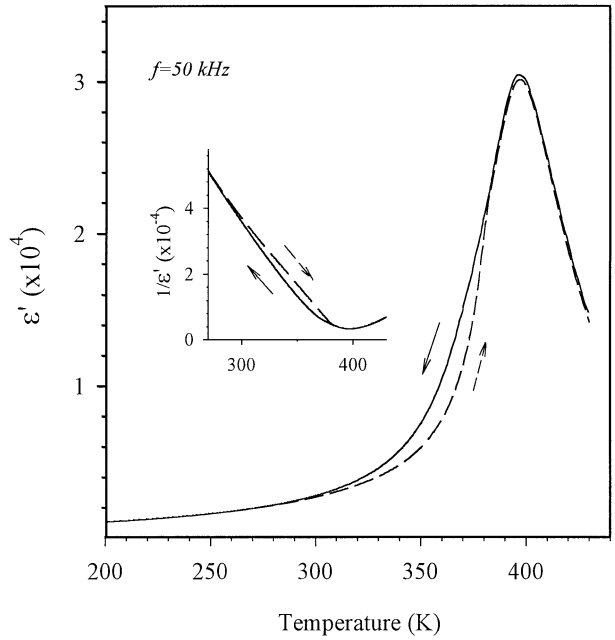

Fig. 4. Thermal hysteresis behaviors of taken at $f = 50$ kHz. The inset is the reciprocal of ε'.

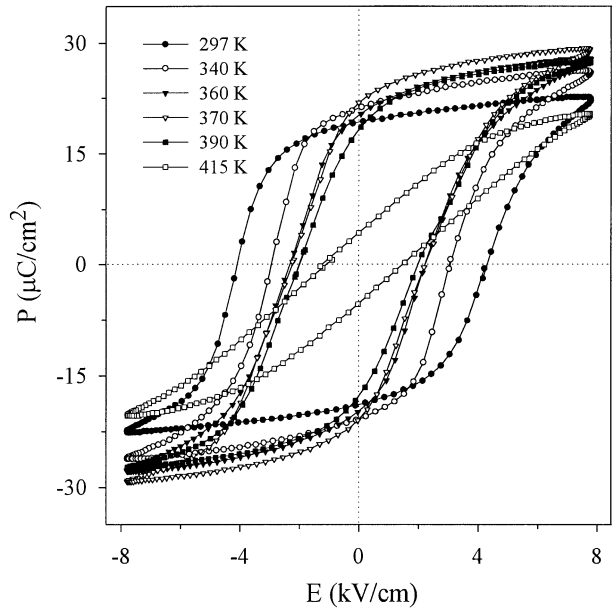

Fig. 5. P–E hysteresis loops obtained upon heating.

Fig. 5. At room temperature, the remanent polarization P_r of PMN–31%PT is about 19 μC/cm^2, and is about the same as the spontaneous polarization P_s defined as the intercept at zero field of the straight-line portion of the hysteresis loop. By comparison, at room temperature, PMN–34%PT[24] has P_s of ~32.5 μC/cm^2, and PT has P_s of 52 μC/cm^5,[25,26] PMN–34%PT exhibits an obvious tetragonal phase near room temperature.[7,24] If one would assume a linear dependence of P_s on PT content, then P_s for PMN–31%PT would be about 31.6 μC/cm^2, i.e. $32.5 - 3 \times (52 - 32.5)/66$. In reality, the PMN–31%PT crystal consists mostly of rhombohedral clusters near room temperature. Accordingly, we assume that P_s has magnitude 31.6 μC/cm^2 for each cluster, and that for large field along {001} the cluster polarizations lie in the four ⟨111⟩

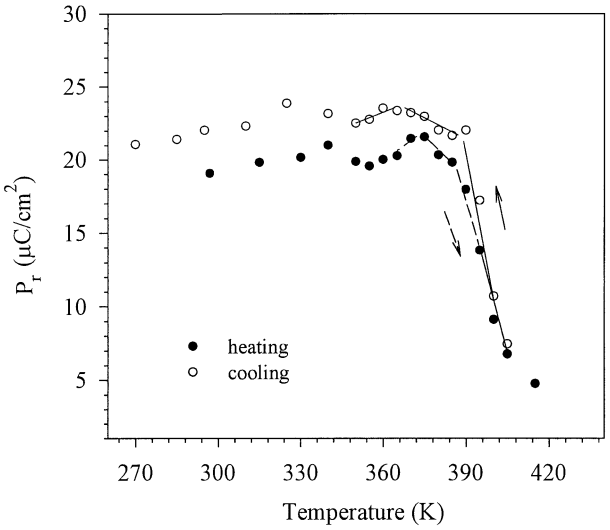

Fig. 6. Temperature dependences of remanent polarization P_r. The solid and dashed lines are guides for the eye.

directions with +1 component along c. Then the net P_s is along c and is reduced by the factor $1/\sqrt{3}$ to 18.2 μC/cm^2, which is close to the measured value of 19 μC/cm^2. The temperature-dependent behavior of remanent polarization P_r is plotted in Fig. 6 and exhibits a thermal hysteresis in a wide temperature range. Instead of the gradual temperature-dependent behavior of polarization in PMN,[27] an abrupt decline was observed near 390 K.

Temperature-dependent domain structures of PMN–31%PT are shown in Fig. 7 upon heating. As shown in the (a) pattern of Fig. 7, domain structures of PMN–31%PT can be distinguished as four regions. Regions "A" and "B" which exhibit optically isotropic background color, possibly correspond to rhombohedral (pseudocubic) clusters. We expect a rhombohedral phase in regions "A" and "B" for two reasons. First, a pure PMN crystal remains optically isotropic without formation of macrodomains and shows pseudocubic symmetry down to very low temperature.[28] Second, according to the MPB location in the phase diagram,[7] PMN–31%PT near room temperature has pseudocubic symmetry with a small rhombohedral distortion.

Regions "C" and "D", which show complex interference patterns, are mostly associated with the rhombohedral phase.[21,22] These inhomogeneous interference patterns are probably caused mostly by clusters or microdomains but partly by macrodomains with deviation of the extinction direction from normal crystallgraphic axes. Such deviation may result from the internal stresses caused by lattice mismatch and domain superposition. Since a pure PMN crystal remains in an optically isotropic pseudocubic state down to very low temperature,[28] interference color domain patterns (in regions "C" and "D") suggest that a long-range FE phase has been triggered by the substitution of 31% Ti^{4+} for the B site complex ions $(Mg_{1/3}Nb_{2/3})^{4+}$. It is believed that the introduction of Ti^{4+} increases the size of local polar domains by strengthening the off-center displacement and enhances the interactions between polar microdomains, leading to a macroscopic symmetry breaking of the pseudocubic state in small portions of the crystal.

With increasing temperature, regions "A" and "B" (Fig. 7) expand their areas and strip-like 90° domain walls begin to appear near 370 K. This indicates that the tetragonal phase begins to develop near 370 K in the crystal. With the dielectric result and the existence of the MPB, the gradual reduction of regions "C" and "D" implies a slowly developing structural transition. Near 380 K, the PMN–31%PT crystal is fully occupied by mutually perpendicular fine domain bands with approximately {110} oriented 90° domain walls appearing as strips. This phenomenon indicates that at 380 K the crystal goes into the tetragonal phase completely. In other words, between 370 and 380 K, the crystal exhibits coexistence of tetragonal and rhombohedral phases. Upon further heating, mutually perpendicular fine 90° domain walls begin to disappear near 400 K and vanish near 420 K. Thus, PMN–31%PT exhibits coexistence of tetragonal and cubic phases between 400 and 420 K, and develops an entirely cubic phase above 420 K.

It was found that different individual domain regions exhibit a large disparity not only in interference patterns, but also in transition temperatures. For instance, upon heating, the area of region "D" (as indicated in Figure 7) exhibits a continuous reduction with the boundary moving to the right side, while the regions "A" and "B" expand their area correspondingly. However, the region "C" exhibits no apparent change up to ~370 K but disappears entirely near 375 K. Upon further heating, similar phenomena were also observed when the crystal transforms from the tetragonal state into the cubic state. Since the MPB depends sensitively on the relative Ti^{4+} occupancy on the B site, these phenomena suggest an inhomogeneous distribution of the Ti^{4+} concentration in the crystal. Such a fluctuation is believed to result from a quenched unequal occupation of the B site by the competitive ions Mg^{2+}, Nb^{5+} and Ti^{4+}. By micro-Brillouin scattering, such microheterogeneity was also detected in the PMN–35%PT crystal.[29] In addition, from direct observation under the polarized light microscope, the width of the 90° domain wall is approximately 0.6 μm in the tetragonal state. However, such a visual estimate may easily be affected by total light reflection at the domain boundary.

What are the physical origins of the temperature-dependent anomalies shown in Figs. 2–7 for PMN–31%PT? For a normal FE phase transition, the transition temperature occurs near where the acoustic phonon frequency has a rapid change. Instead of a sharp softening, the acoustic phonon frequency (Fig. 2) of PMN–31%PT shows a gradual decline and reaches a broad minimum dip near 395 K. A similar acoustic anomaly was seen in pure PMN.[30] The real part ε' of dielectric permittivity (Fig. 3) exhibits a broad frequency-dependent behavior with maxima located near 400 K. This value is reasonably consistent with the temperature ~405 ± 5 K (cubic PE ↔ tetragonal FE phases) predicted in ref. 7. In addition, a weak thermal hysteresis of the permittivity (Fig. 4) was observed in the region of ~390–400 K. A broad damping maximum (Fig. 2) which has often been seen in other mixed crystals,[30] was observed near 395 K. Such a damping anomaly reveals that order parameter fluctuations originating from competition between local symmetries are the dominant dynamic mechanism as the system approaches the phase transition. One can expect that the gradual softening anomaly of the phonon frequency (Fig. 2) is associated with fluctuations of coupled local domains. As evidenced in Fig. 7, the

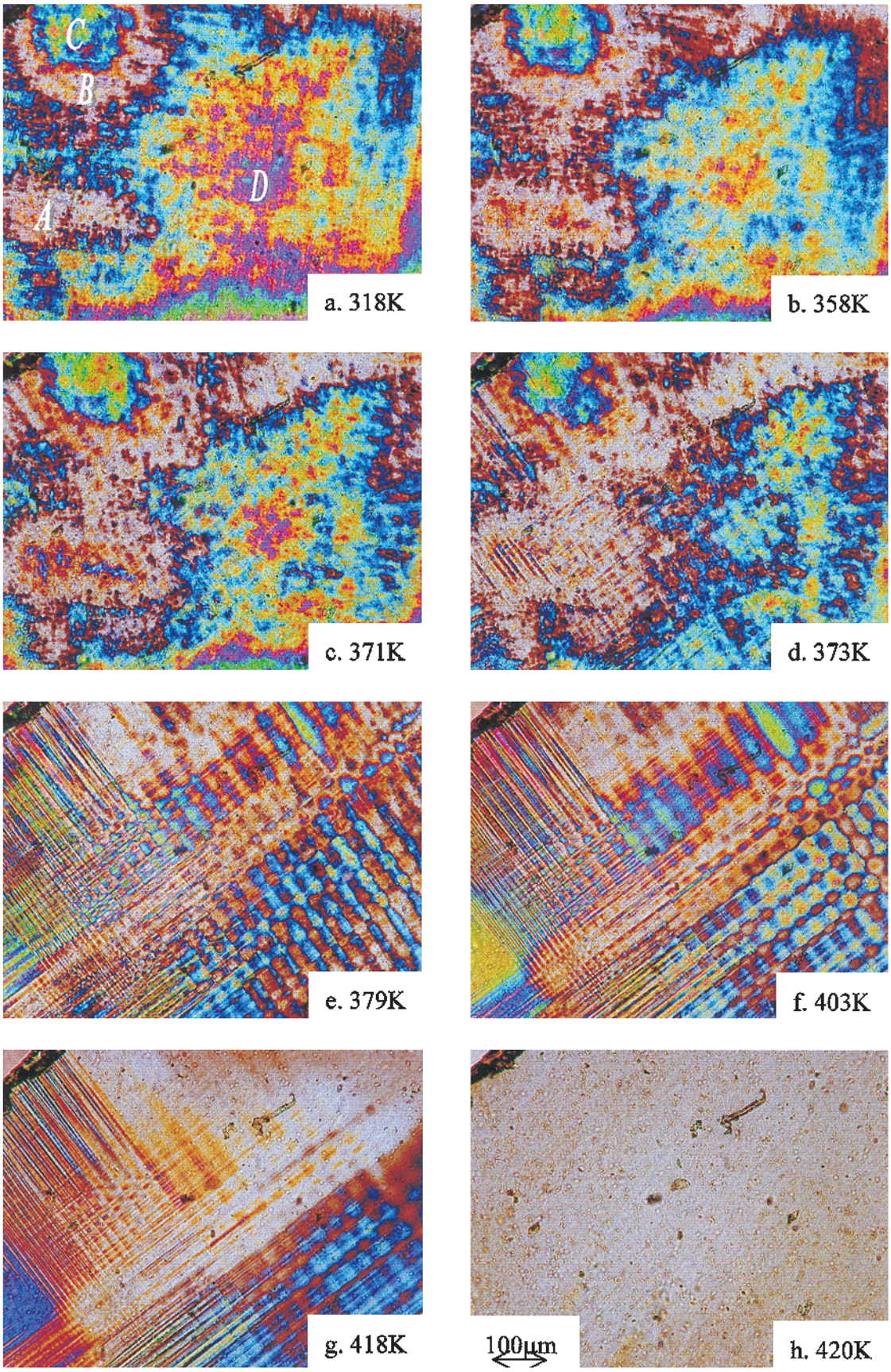

Fig. 7. Domain structures observed on a {001} oriented platelet upon heating. "A-D" indicate individual domain regions obtained at 318 K.

isotropic cubic state begins to develop near 400 K and occupies the crystal entirely near 420 K. Thus, between ~400 K and ~420 K, PMN–31%PT undergoes a diffuse phase transition from the tetragonal FE phase to the cubic PE phase. In other words, the crystal exhibits a coexistence of tetragonal and cubic phases in the region of ~400–420 K.

FE phase transitions are known to be associated with a crystal lattice soft mode. If the transition is strongly first-

order, mode softening may not be detectable. We note that a zone-center ($q = 0$) acoustic soft mode in the reduced Brillouin zone of the reciprocal sublattice always has, for a normal second-order transition, a zero frequency on approaching the transition temperature from the ordered phase. Therefore, the nonzero minimum of the phonon frequency (near 395 K) in PMN–31%PT implies either a weak first-order transition or that the structural instability must be coupled with other mode(s), perhaps the transverse optical (TO) phonon mode. In other words, what might be happening is that above the transition temperature the TO mode has too high a frequency to affect the LA mode. Then on approaching the transition temperature, the TO mode has a frequency of the order of the LA phonon frequency, which produces relaxation of the LA mode through biquadratic coupling. In cubic perovskites, the average structure does not permit linear coupling to an acoustic mode. Finally, on further cooling, the TO mode freezes below the LA phonon frequency, and the effect of the coupling disappears again. On the other hand, the gradual softening behavior (Fig. 2) associated with a broad minimum dip, implies strong order parameter fluctuations between coupled local clusters.

In the lower temperature region, as shown in Figs. 2 and 3, both the ε' and ε'' of PMN–31%PT exhibit an extra shoulder near 380 K with frequency dispersion. An obvious thermal hysteresis was also observed in the region of ~300–380 K. As revealed in Figure 7, mutually perpendicular 90° domain walls begin to appear near 370 K and completely occupy the crystal near 380 K. Thus, the extra dielectric shoulder near 380 K must correlate to establishment of the long-range FE tetragonal state. Based on the above results, one can conclude that the PMN–31%PT crystal undergoes a first-order diffuse phase transition (rhombohedral FE $\rightarrow$ tetragonal FE) from ~370 K to ~380 K. In other words, PMN–31%PT exhibits a coexistence of rhombohedral and tetragonal phases in the region of ~370–380 K. Similar coexistence of rhombohedral and tetragonal symmetries was observed in another relaxor-based FE crystal $(PbZn_{1/3}Nb_{2/3}O_3)_{0.9}(PbTiO_3)_{0.1}$ (PZN–10%PT) near the MPB.[6] We call this a first-order transition for two reasons. First, the thermal hysteresis in the dielectric permittivity shows that the system is metastable in this temperature region. Metastability can occur for first- but not second-order transitions. Second, the point groups of the tetragonal and rhombohedral symmetries do not have a group-subgroup relation, so a transition between these phases must be of first order. The usual distinctions between first- and second-order transitions, such as discontinuity in dP/dT, do not apply for diffuse phase transitions.

Probably the most convincing evidence for the FE nature of PMN–31%PT is the extra peak in the zero-field-heated (ZFH) dielectric permittivity seen after field cooling (FC) in a dc bias field ($E = 4$ kV/cm) to the domain state. The extra peak superimposed on the broad background of dielectric permittivity is clearly evident at 370 K. The temperature for this anomaly (but not its amplitude) is independent of frequency. A similar field-induced dielectric anomaly has been observed in the PMN system.[3,31] By heating the PMN crystal in a dc electric field, a long-range FE phase transition associated with an extra dielectric peak at $T_c \sim 212$ K, was found and is attributed to the percolating cluster caused by the suppression of the random fields originating from charged compositional fluctuations at the B site.[3] It is well known that in relaxor ferroelectrics the highly sensitive local polar states are easily affected by external perturbations. Contrary to normal ferroelectrics, an external electric field may enhance the interactions between local polar microclusters and induces marked changes.[4,32] Thus, it is reasonable to expect that the extra peak at 370 K in the FC-ZFH dielectric permittivity of PMN–31%PT can be attributed to the establishment of a long-range percolating FE cluster during the FC process. In addition, the broad dispersive permittivity peak following FC has magnitude about 17,000 (Fig. 8), about 40% lower than the 30,000 value shown in Figure 3 for ZFC. Perhaps the FC process induces domain reorientations, and hence reduces the domain wall contributions to the dielectric permittivity. Another possibility is that this reduction could be a consequence of partial poling of the network of nonpercolating FE clusters by the external electric field.

To characterize the temperature dependence of the dielectric permittivity above T_m, we fitted the experimental data to the empirical formula,[33–35]

$$\frac{\varepsilon'_m}{\varepsilon'(f,T)} = 1 + \frac{[T - T_m(f)]^\gamma}{2\delta_\gamma^2} \tag{1}$$

where ε'_m corresponds to the maximum value of the dielectric permittivity at T_m. The value of γ ($1 \le \gamma \le 2$) is the expression of the degree of dielectric relaxation for relaxor-based FE materials. When $\gamma = 1$, eq. (1) expresses Curie-Weiss behavior, while for $\gamma = 2$, eq. (1) is identical to Smolensky's formula.[36] The parameter δ_γ has been used as a measure of degree of diffuseness for the diffuse phase transition. Based on eq. (1), δ_γ can be determined from the slope of the $\varepsilon'_m/\varepsilon'$ vs $(T - T_m)^\gamma$ dependence, which is linear. Figure 9 shows the plot of $\varepsilon'_m/\varepsilon'$ vs $(T - T_m)^\gamma$. The solid and dashed lines are the best fits of eq. (1) to the dielectric data obtained at measuring frequencies 50 kHz and 1 MHz, respectively. The fitting parameters are $\gamma = 1.73$, $\delta_\gamma = 13.8$ (for 50 kHz), and $\delta_\gamma = 13.6$ (for 1 MHz). It was found that the experimental data in the temperature region $T_m \le T \le T_m + 30$ K obey the empirical eq. (1) quite well. The parameter δ_γ shows a weak tendency to change with frequency. Also, no correla-

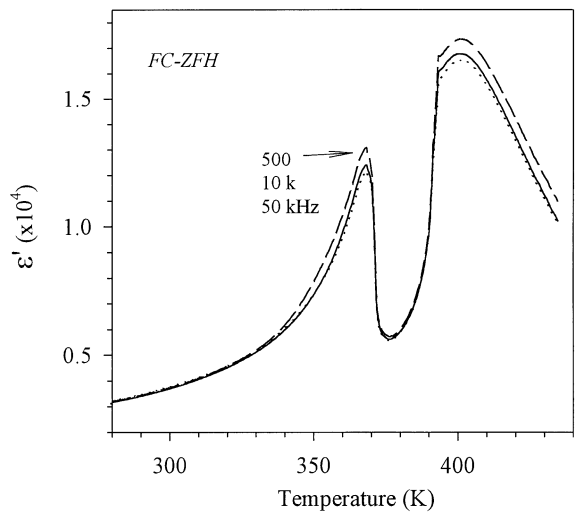

Fig. 8. Temperature dependence of ε' for frequencies 10–100 kHz, obtained from the FC-ZFH process.

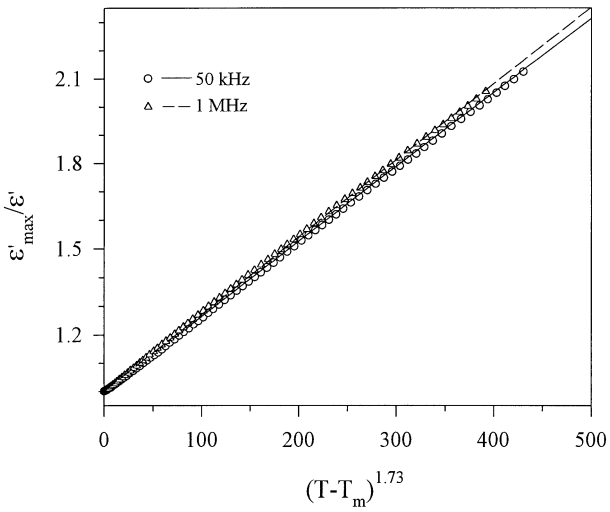

Fig. 9. $\varepsilon'_m/\varepsilon'$ vs $(T - T_m)^\gamma$ for data obtained at frequencies 50 kHz and 1 MHz. The solid and dashed lines are fits of eq. (1).

tion between the parameter γ and measuring frequency was found. Bokov *et al*. recently demonstrated that, in both PMN and PMN–25%PT, the dielectric permittivity ε' obeys the relation $\varepsilon'_A/\varepsilon' = 1 + (T - T_A)^2/2\delta_A^2$ in a wide temperature range above T_m.[37,38] However, this empirical quadratic law did not fit better than eq. (1) for the dielectric data of the PMN–31%PT system. The possible reason is that both PMN and PMN–25%PT do not have a morphotropic phase boundary (MPB).[7] In other words, PMN–25%PT has a phase transition (cubic ↔ rhombohedral) and dielectric behavior similar to those of pure PMN. It is well known that the dielectric permitivity of PMN was fitted perfectly by the quadratic law.[36–38] On the other hand, the PMN–31%PT crystal has a morphotropic phase boundary and goes through successive phase transition (cubic ↔ tetragonal ↔ rhombohedral) as temperature changes.[7] Nevertheless, we need to admit that the search to find an universal empirical formula describing the temperature dependence of ε' in the vicinity of the so-called diffuse phase transition is still open.

4. Conclusions

From the temperature-dependent behaviors of acoustic phonon spectra, dielectric permittivities, *P–E* hysteresis loops and domain structures, it was found that PMN–31%PT undergoes successive phase transitions. Below ~370 K, PMN–31%PT exhibits a rhombohedral (pseudocubic) FE phase. A coexistence of rhombohedral and tetragonal phases was observed in the region of 370–380 K. Above 380 K, the PMN–31%PT crystal goes entirely into the tetragonal phase characterized by strip-like 90° domain walls. Upon further heating, mutually perpendicular 90° domain walls begin to disappear near 400 K and vanish near 420 K. In other words, PMN–31%PT has another coexistence region, of tetragonal and cubic phases, between 400 and 420 K, and develops an isotropic cubic phase above 420 K. In addition, individual domain regions have different transition temperatures. This phenomenon suggests an inhomogeneous distribution of Ti^{4+} concentration in the crystal. It is believed that this spatial fluctuation of Ti^{4+} content results from an unequal occupation of the B-site by the competitive ions Mg^{2+}, Nb^{5+} and Ti^{4+} while the lattice structure is established.

In the FC-ZFH process, an extra dielectric peak was observed at 370 K and is attributed to the establishment of a percolating polar cluster induced by the external electric field. The magnitude of the broad dispersive permittivity peak following FC is reduced about 40%. This reduction is probably due to domain reorientations or partial poling of the network of nonpercolating FE clusters. The thermal hysteresis behavior of dielectric permittivity implies that the phase transitions near 380 K and 400 K are both first-order. Unlike normal ferroelectrics whose dielectric permittivity above the Curie point follows the Curie-Weiss law $1/\varepsilon = (T - T_{cw})/C$, the dielectric permittivity ε' of PMN–31%PT obeys the empirical relation, $\varepsilon'_m/\varepsilon'(f, T) = 1 + [T - T_m(f)]^\gamma/2\delta_\gamma^2$, in a wide temperature range above T_m.

Acknowledgments

This work was supported by Grant No. NSC89-2112-M-030-006 (R.O.C.) and DOD EPSCoR Grant No. N00014-99-1-0523 (USA).

1) L. E. Cross: Ferroelectrics **76** (1987) 241.
2) D. Viehland, M. Wuttig and L. E. Cross: Ferroelectrics **120** (1991) 71.
3) V. Westphal, W. Kleemann and M. D. Glinchuk: Phys. Rev. Lett. **68** (1992) 847.
4) Z.-G. Ye: Key Eng. Mater. **155–156** (1998) 81.
5) L. A. Shebanov, P. Kaspostins and J. Zvirgzds: Ferroelectrics **56** (1984) 1057.
6) M. L. Mulvihill, S. E. Park, G. Risch, Z. Li and K. Uchino: Jpn. J. Appl. Phys. **35** (1996) 3984.
7) T. R. Shrout, Z. P. Chang, N. Kim and S. Markgraf: Ferroelectr. Lett. **12** (1990) 63.
8) D. S. Paik, S. E. Park, S. Wada, S. F. Liu and T. R. Shrout: J. Appl. Phys. **85** (1999) 1080.
9) M. K. Durbin, E. W. Jacobs, J. C. Hicks and S.-E. Park: Appl. Phys. Letter **74** (1999) 2848.
10) U. Belegundu, X. H. Du and K. Uchino: Ferroelectrics **222** (1999) 67.
11) S.-E. Park and T. R. Shrout: J. Appl. Phys. **82** (1997) 1804.
12) Y. Yamashita: Jpn. J. Appl. Phys. **33** (1994) 5328.
13) S. W. Choi, T. R. Shrout, S. J. Jang and A. S. Bhalla: Ferroelectrics **100** (1989) 29.
14) R. F. Service: Science **275** (1997) 1878.
15) H. Luo, G. Xu, P. Wang and Z. Yin: Ferroelectrics **231** (1999) 97.
16) H. Fu and R. E. Cohen: Nature **403** (2000) 281.
17) C.-S. Tu, F.-C. Chao, C.-H. Yeh, C.-L. Tsai and V. H. Schmidt: Phys. Rev. B **60** (1999) 6348.
18) S. Gentil, G. Robert, N. Setter, P. Tissot and J.-P. Rivera: Jpn. J. Appl. Phys. **39** (2000) 2732.
19) M. K. Durbin, J. C. Hicks, S.-E. Park and T. R. Shrout: J. Appl. Phys. **87** (2000) 8159.
20) S. Saitoh, T. Kobayashi, K. Harada, S. Shimanuki and Y. Yamashita: Jpn. J. Appl. Phys. **37** (1998) 3053.
21) Z.-G. Ye and M. Dong: J. Appl. Phys. **87** (2000) 2312.
22) F. Jona and G. Shirane: *Ferroelectric Crystals* (Dover, New York, 1993) Chap. IV, pp. 160–167.
23) C.-S. Tu, R. S. Katiyar, V. H. Schmidt, R. Guo and B. S. Bhalla: Phys. Rev. B **59** (1999) 251.
24) F.-C. Chao: M. S. Thesis: Fu Jen University, Taiwan, Republic of China, 2000.
25) J. P. Remeika and A. M. Glass: Mater. Res. Bull. **5** (1970) 37.
26) E. C. Subbarao: Ferroelectrics **5** (1973) 267.
27) V. A. Bokov and I. E. Mylnikov: Sov. Phys. Solid State **3** (1961) 613.
28) Z.-G. Ye and H. Schmid: Ferroelectrics **145** (1993) 83.
29) F. M. Jiang and S. Kojima: Appl. Phys. Lett. **77** (2000) 1271.
30) C.-S. Tu, V. H. Schmidt and I. G. Siny: J. Appl. Phys. **78** (1995) 5665.
31) R. Sommer, N. K. Yushin and J. J. van der Klink: Phys. Rev. B **48** (1993) 13230.
32) O. Bidault, M. Licheron, E. Husson, G. Calvarin and A. Morell: Solid State Commun. **98** (1996) 765.

33) H. T. Martirena and J. C. Burfoot: Ferroelectrics **7** (1974) 151.
34) Z. Y. Cheng, R. S. Katiyar, X. Yao and A. Guo: Phys. Rev. B **55** (1997) 8165.
35) K. Uchino and S. Nomura: Ferroelectrics Lett. **44** (1982) 55.
36) G. A. Smolensky: J. Phys. Soc. Jpn. **28** (1970) Suppl. p. 26.
37) A. A. Bokov and Z.-G. Ye: Solid State Commun. **116** (2000) 105.
38) A. A. Bokov and Z.-G. Ye: Appl. Phys. Lett. **77** (2000) 1888.